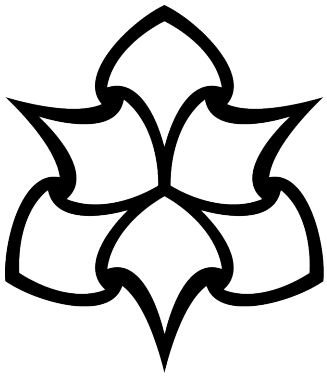

CCP-WSI Blind Test Series 3: OpenFOAM Simulation of Focused Wave Interaction with a Simplified Wave Energy Converter

Hao Chen, Ling Qian, Zhihua Ma, Wei Bai and Zaibin Lin
Centre for Mathematical Modelling and Flow Analysis, School of Computing, Mathematics and Digital Technology
Manchester Metropolitan University, Manchester, United Kingdom

ABSTRACT

This paper presents a numerical study of a simplified wave energy converter (WEC) with and without a moon-pool under focused wave conditions and the work presented corresponds to a contribution to the CCP-WSI Blind Test Series 3. The numerical model applies the overset mesh technique in order to deal with large amplitude motions induced by the focused wave groups. The generation of the incident wave group is first examined through a mesh convergence test and by comparing with the experimental data. Simulations are then carried out with the presence of the WEC. In total three wave conditions are considered, each with the same wave period but different wave height. Non-linear effects on the WEC motion are clearly shown when the wave steepness increases and wave over-topping occurs. Furthermore, the effects of the moon pool on the dynamics and kinematics of the WEC including the damping effects on pitch response are also discussed, where the WEC motion is compared for the case with and without a moon-pool under the same wave conditions.

KEY WORDS: Wave energy converter; Overset mesh; Floating body; Focused wave groups, CCP-WSI Blind Test Series 3.

INTRODUCTION

In recent years, the possibility of harnessing energy from ocean waves has gained great interests, where different design concepts of wave energy converters (WECs) have been proposed, such as oscillating water columns, bottom-hinged pitching devices, floating pitching devices, over-topping devices, and point absorbers.

Point absorbers are one of the simplest WECs. Their characteristic length is generally shorter than typical wave length at the peak wave frequency and they are typically subjected to large amplitude motions close to resonance. Under such conditions, highly nonlinear wave-structure interaction will normally occur, which cannot be predicted accurately by simple models based on linear or second order potential flow theory. Hereby the fully nonlinear numerical models such as those base on the solutions of the full Navier-Stokes equations are needed. Examples of fully nonlinear CFD simulations on the point absorbers and other types of WECs have been presented in Yu and Li (2013), Palm et al. (2016), Hu et al. (2011), Qian et al. (2005) and Ransley (2017).

Marine operations from ships and offshore platforms often use moon-pools to lower or lift devices such as subsea modules and remote operated underwater vehicles. Piston-mode resonance can be excited by the relative vertical motions in the neighbourhood of the moon-pool, which causes strong amplification of the dynamic wave elevation in the moon-pool. This has been studied in e.g. Fredriksen et al. (2014), Fredriksen et al. (2015) and Faltinsen et al. (2007).

In the present work, the motion responses of a point absorber under focused wave groups are numerically simulated. Two geometries of the simplified WEC are considered, namely a hemispherical-bottom cylinder and a hollow cylinder with moon-pool. The motion responses of the WEC under different wave conditions are compared with the effects of moon-pool investigated. The test cases, which are proposed by the CCP-WSI Blind Test Series (Ransley et al 2019) in conjunction with the Annual ISOPE Conferences, are designed to provide an understanding of the required model fidelity for modelling the behaviour of floating structures, for which this work provides a reasonably high fidelity contribution.

NUMERICAL MODEL

Flow Solver

The incompressible Navier-Stokes equations are solved in the open-source toolbox OpenFOAM for a two-phase system, where volume of fluid method is employed to capture the free surface. The governing equations for this system are given as:

$$\nabla \cdot \boldsymbol{u} = 0 \tag{1}$$

$$\frac{\partial \rho \boldsymbol{u}}{\partial t} + \nabla \cdot (\rho \boldsymbol{u}\boldsymbol{u}) - \nabla \cdot \mu \nabla \boldsymbol{u} = -\nabla p^* - (\boldsymbol{g} \cdot \boldsymbol{x}) \nabla \rho \tag{2}$$

$$\frac{\partial \alpha}{\partial t} + \nabla \cdot (\boldsymbol{u}\alpha) + \nabla \cdot (\boldsymbol{u}_r \alpha (1-\alpha)) = 0 \tag{3}$$

where $\boldsymbol{x} = (x, y, z)$ is the Cartesian coordinate system, $\boldsymbol{u}$ is the velocity, $\boldsymbol{g}$ is the gravitation, ρ is the density, μ is the dynamic viscosity and p^*

is the pseudo-dynamic pressure, where the hydrostatic pressure has been subtracted. $\boldsymbol{u}_r$ here is referred as the compressive velocity (Berberovic et al., 2009), which aids in retaining a sharp interface. The term $\alpha(1-\alpha)$ vanishes everywhere except at the interface.

Rigid body motion solver

The standard OpenFOAM sixDoFRigidBodySolver is used to solve the six degrees of freedom motion solver, where the mooring system is modelled as a linear spring. Linear and angular momentum conservation equation is solved to obtain the accelerations. The acceleration is under-relaxed with a fixed factor of 0.4 to maintain the stability of the solver. Then Newmark scheme is used to numerically integrate the acceleration in order to calculate the displacement and the velocity.

Overset mesh

The overset mesh functionality released in OpenFOAM v1706 (ESI version) is applied to properly resolve the moving mesh issues. Under extreme sea conditions, the motion of the floating structures can be eventually very large, which is not straightforward to model using the dynamic mesh approach. The overset mesh can effectively resolve this issue since it adopts a composite mesh structure. We shall use two layers of mesh, namely the background mesh and the body fitted mesh. The background mesh is fixed, while the body-fitted mesh follows the motion of the floating structure without any deformation. Data are exchanged at every time step between these two layers of mesh.

Numerical wave generation

The extreme wave conditions are described by NewWave type focused wave groups. The wave generation toolbox IHFOAM, developed by Higuera et al. (2013), is employed to numerically generate the focused wave groups. Unlike the moving paddles or flaps used in physical modelling in wave tanks, the surface elevation and the particle velocity profiles at the fixed wave generation boundary are calculated based on the second order irregular wave theory, which have been given in e.g. Hu et al. (2016).

RESULTS AND DISCUSSION

Experiments

The experiments, as part of the CCP-WSI project for the CCP-WSI Blind Test Series 3, were performed in the COAST Laboratory Ocean Basin at Plymouth University, UK. The basin is 35 m long and 15.5 m wide. The depth of the basin was set to 3 m in this set of experiments. Two types of wave energy converters were considered in the experiments, namely the simple hemispherical-bottomed cylinder and a cylinder with a moon-pool, as shown in Fig. 1 and Fig. 2, respectively. Their mass properties are given in Table 1. The WECs were moored by a linear spring vertically which connects to the basin bottom. The spring stiffness was 67 N/m and the pretension force on the mooring lines were 32.07 N and 31.55 N for the two cases.

Table 1 Mass properties for the WECs. M is the mass, I is the moment of inertia. ID is the case ID number. Case 1 is for the hemispherical-bottom cylinder in focused wave groups and Case 2 is the hollow cylinder with moon-pool in focused wave groups.

ID	M [kg]	I_{xx} [kgm^2]	I_{yy} [kgm^2]	I_{zz} [kgm^2]
1	43.674	2.219	2.219	1.143
2	61.459	1.790	1.790	3.298

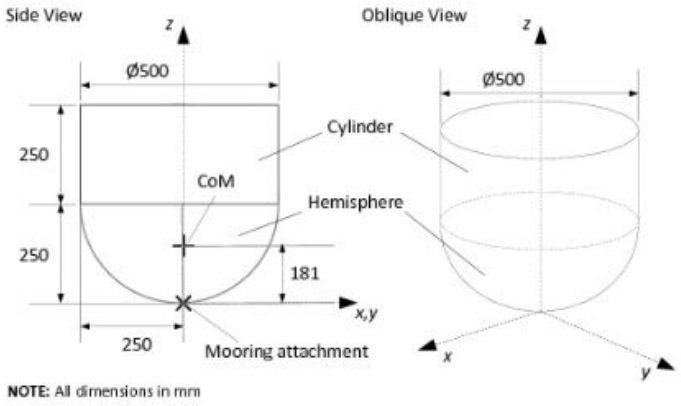

Fig. 1 The geometry and the dimensions for the hemispherical-bottom cylinder. CoM is the centre of mass. (Reproduced from the CCP-WSI Blind Test Series 3 description)

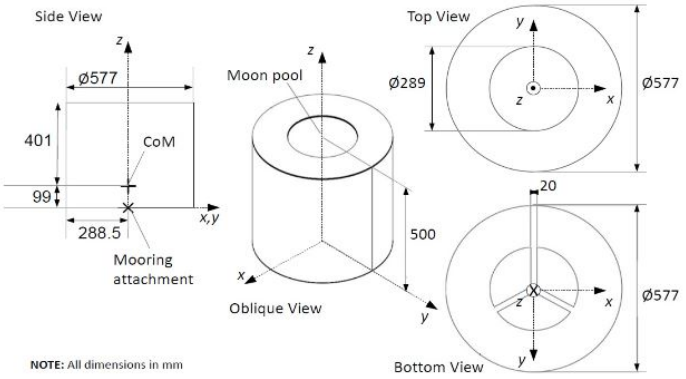

Fig. 2 The geometry and the dimensions for the hollow cylinder with a moon-pool. CoM is the centre of mass. (Reproduced from the CCP-WSI Blind Test Series 3 description)

The wave parameters for the incident wave groups are given in Table 2. All the wave groups were crest-focused with the same peak frequency but increasing wave steepness. Each wave was created using linear superposition of 244 wave fronts with frequencies evenly spaced between 0.10 Hz and 2 Hz. For all cases, 13 wave gauges were placed in the wave basin as illustrated in Fig. 3. Gauge 5 was placed at the rest position of the buoy(s) (with the structure in place this wave gauge was removed but the same number system maintained), which also corresponds to the focal position of the wave group.

Table 2 The test conditions for the incident wave groups. All the waves were generated based on the PM spectrum. A is the focal crest height, T_p is the wave period for the wave component at peak frequency, H_s is the significant wave height and k_p is the wave number for the wave component at the peak frequency.

Case	A [m]	T_p [s]	H_s [m]	h [m]	k_pA [-]
1	0.20	2.5	0.274	3.00	0.1287
2	0.30	2.5	0.274	3.00	0.1931
3	0.32	2.5	0.274	3.00	0.2060

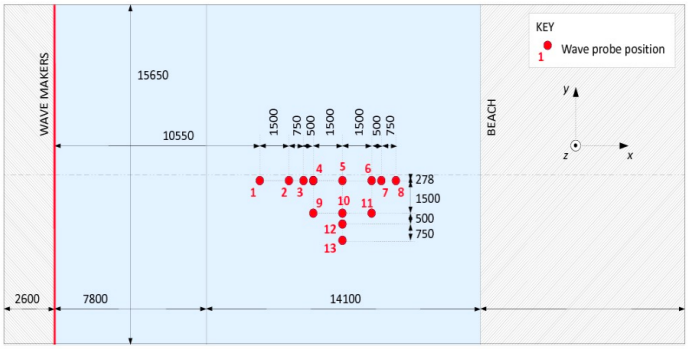

Fig. 3 The positions of the wave gauges around the WECs. (Reproduced from the CCP-WSI Blind Test Series 3 description)

Computational domain and mesh

A domain size of 20 m long and 6 m wide is used throughout the simulations, where the domain length corresponds to $1.9\lambda_p$ where λ_p is the wave length at the peak wave frequency, and the domain width is equal to about $12D_1$ and $10D_2$ where D_1 and D_2 are the diameter of the WEC without and with moon pool, respectively. The depth of the wave tank is set to the same as in the experiments, i.e. 3 m, while the height above the water surface is 1 m to allow the two-phase flow simulation. The wave groups are focused at 12 m from the wave-maker side at 12 s. As the overset mesh is applied in the numerical model, two layers of mesh are used. Hexahedra cells are applied in the background mesh, which are static throughout the simulation. The cells are stretched vertically from the bottom and the atmosphere boundary to the free surface area between $z = -0.3$ and $z = 0.3$ ($z = 0$ corresponds to the still water level) and they are uniformly distributed in this area. In x and y direction, the mesh cells are also stretched smoothly to the focal position. Regarding the body-fitted mesh layer, the utility snappyHexMesh is used to cut the regular hexahedra cells into tetrahedron. Moreover, the mesh is further refined near the WEC body surface. An example of the overset mesh near the WEC is presented in Fig. 4.

Incident wave groups

Convergence tests

Convergence study is carried out to examine the sensitivity of mesh resolution on the generated incident wave groups. The domain size is the same as the background mesh introduced above. Only the wave case with the lowest crest height (case 1) was tested here as a finer mesh is required to resolve the free surface for smaller waves. Three mesh resolutions are used in the study, of which the parameters are shown in Table 3. The CPU time shown in the table is the wall clock time of running the test case on two Intel Xeon E5-2600 CPUs with 32 cores. The surface elevation at the focal position (Gauge 5) is plotted in Fig. 5 using these mesh resolutions. It is observed that the time series of the surface elevations are almost identical, which perfectly collapse into one line. This demonstrates that the mesh resolutions are sufficiently fine and the numerical solutions are convergent. Grid 2 will be used in the following simulations.

Comparison of surface elevation

We present comparison of the surface elevation at several wave gauges for Case 1 and Case 3 in Fig. 6 and Fig. 7. The selected wave gauges are along the centre line from the front to the back part. It is observed that the numerical results agree well with the experimental data for Case 1, corresponding to the relatively mild wave conditions. However, when the

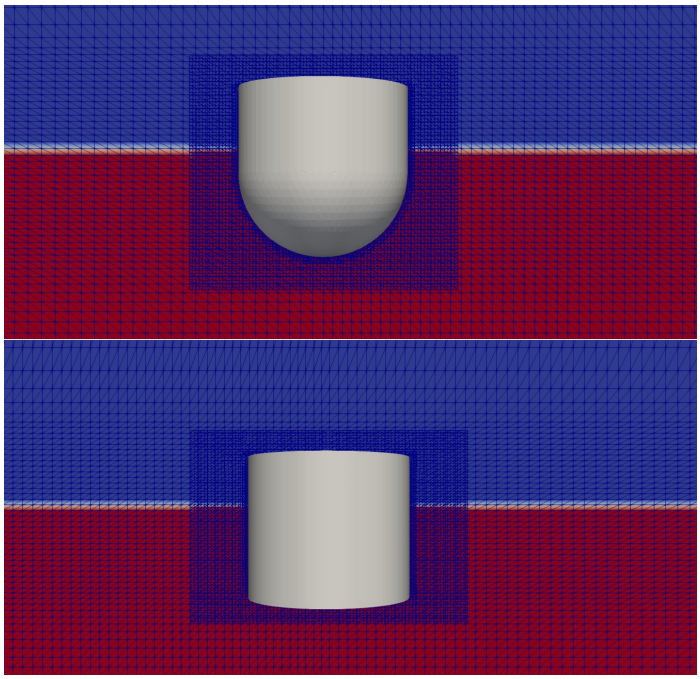

Fig. 4 An example of the overset mesh near the WEC for the case without moon pool (upper) and with moon pool (lower).

Table 3 The grid parameters in the convergence study. Δx, Δy and Δz are the averaged cell length in x, y and z directions in the refined free surface area.

ID	Δx [m]	Δy [m]	Δz [m]	NO. [-]	CPU time [hour]
1	0.076	0.077	0.025	1.64 m	4.67
2	0.060	0.061	0.020	3.22 m	11.43
3	0.050	0.051	0.017	5.56 m	16.08

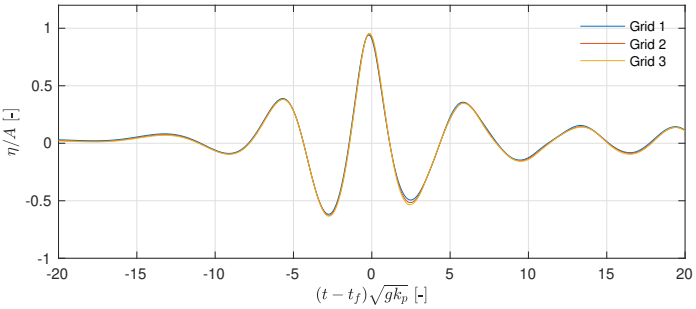

Fig. 5 The surface elevation at WG 05 using different mesh resolutions.

wave steepness is increasing, the deviation is likely to increase. At the focal position (WG05), the wave crest is underpredicted by the numerical model for about 26%.

Effects of wave height on the WEC motion

The surge, heave and pitch motion of the wave energy converter with moon pool are presented in Fig. 8 under three different wave conditions. We only plot the numerical results, since the experimental data are not available yet. Several comments are given here for the numerical results. Regarding the surge motion, strong drift motion is found for the cases with wave conditions 2 and 3. The maximum surge motion is more than

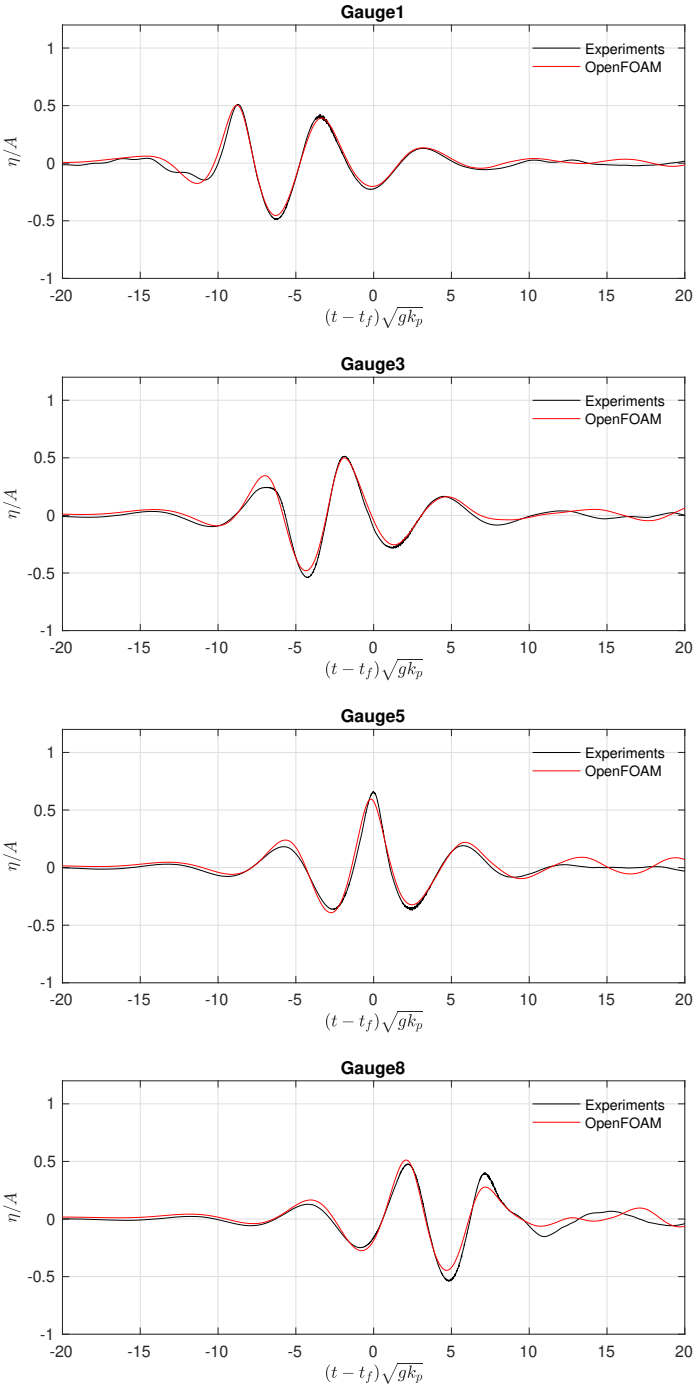

Fig. 6 Comparison of surface elevation at the selected wave gauges for Case 1.

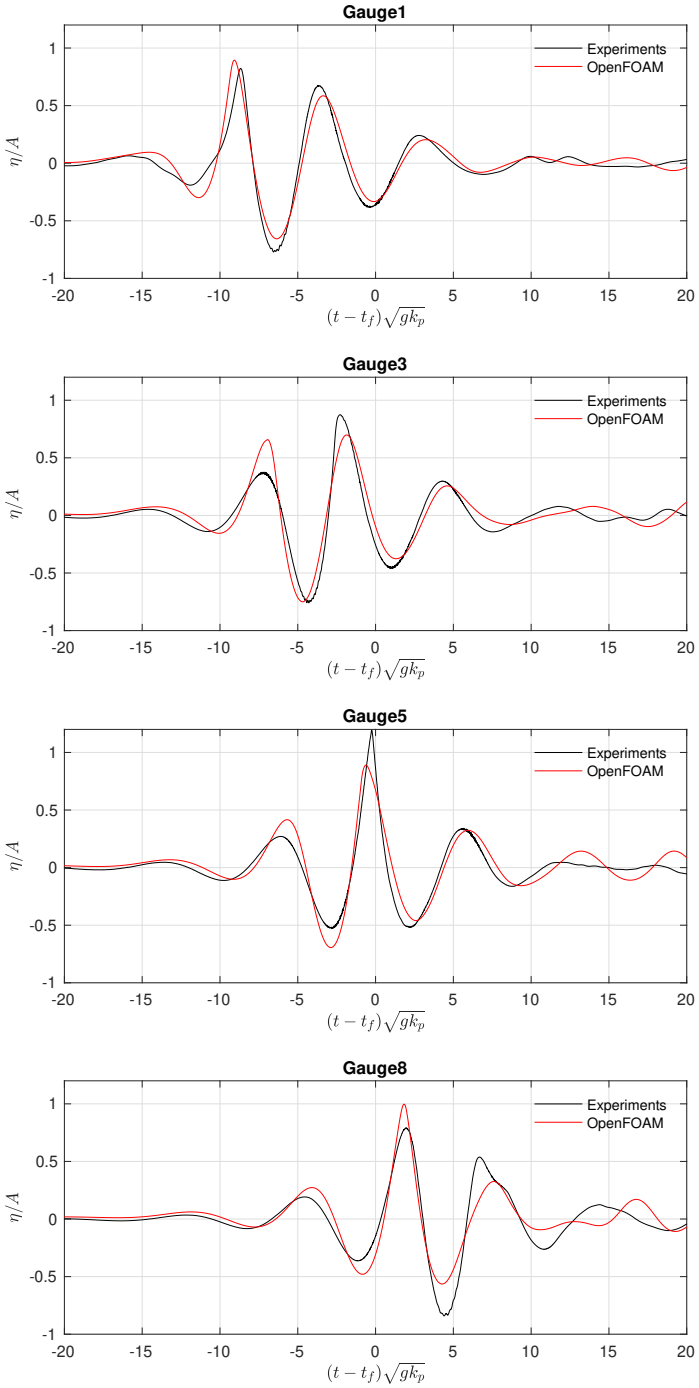

Fig. 7 Comparison of surface elevation at the selected wave gauges for Case 3.

five times the wave crest. This may be partially due to the mooring system. A single point mooring line may not provide sufficient restoring force. Under relatively large wave steepness, it takes particularly long time to restore to the original position. Meanwhile, it is also possible that the numerical model is not stable enough, leading to the drift motion.

Regarding the heave motion, the nondimensional crest is quite similar for all the cases, i.e. smaller than 1. But a second peak is observed for Case 2 and 3. This is due to the strong nonlinear free surface motion, where violent overtopping occurs. A snapshot of the free surface motion at different time instants near the focal time is presented in Fig. 9. The near field waves are clearly diffracted and radiated due to the presence of the WEC. Clear overtopping of incident waves are generated at t = 12.80 and t = 13.00 s.

Effects of moon-pool on the WEC motion

The three motion modes of the WEC with and without moon-pool is plotted in Fig. 10 for wave condition 1. A strong dissipation effect is

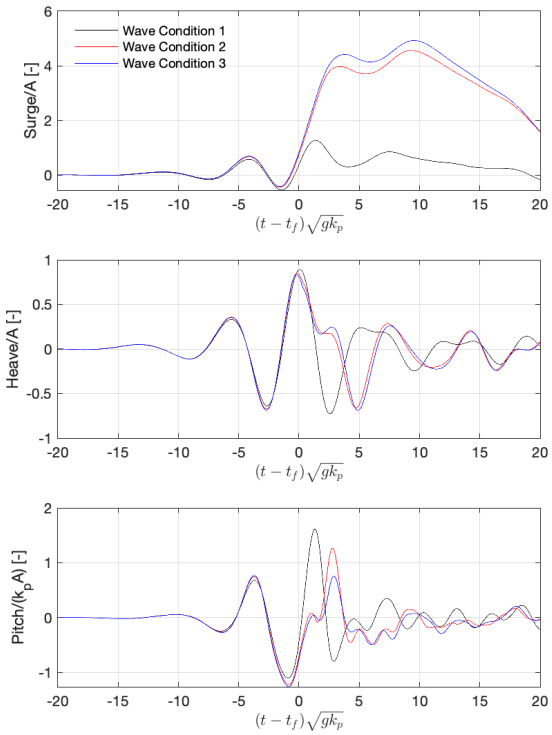

Fig. 8 The surge, heave and pitch motion of the WEC under three wave conditions for the case with moon-pool.

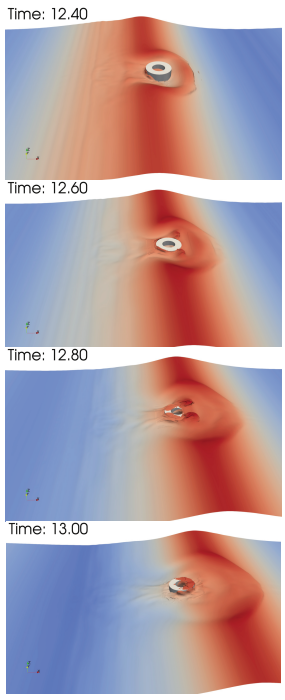

Fig. 9 The free surface motion near the WEC with moon-pool under wave condition 3.

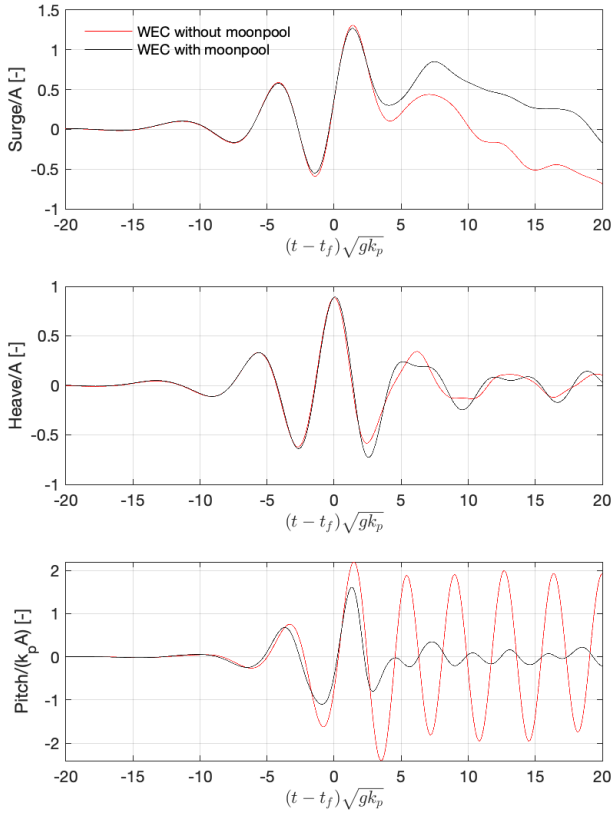

Fig. 10 The surge, heave and pitch motion of the WEC with and without moon pool under wave condition 1.

found when the WEC is equipped with moon pool, due to the internal fluid motion inside the moon-pool. This is particularly obvious for the pitch motion. When the WEC is equipped with moon pool, the crest value of the pitch motion is smaller than the case without moon-pool. Furthermore, the pitch motion is soon damped in the defocusing process for the case with moon-pool, while it keeps oscillating for the other case. Similar phenomenon is found for the surge motion in the de-focusing process. But the crest value is the same for both cases. Moreover, for heave motion, the moon-pool effect is rather small, and the heave motion exhibits similar characteristics for both cases. This is reasonable since the dissipation of the moon-pool is likely due to the viscous effects, while the heave motion is primarily dominated by the potential energy of the waves.

CONCLUSIONS

This paper presents the numerical modelling of a simplified WEC with and without a moon-pool under focused wave groups as a contribution to the CCP-WSI Blind Test Series 3. The numerical model applies an overset mesh method in order to consider the large amplitudes motions induced by the waves. Three wave conditions with increasing wave steepness are tested and from the simulation results, it is clear that the motion of the WEC becomes strongly nonlinear when the non-dimensional wave steepness k_pA reaches 0.2. When comparing the WEC motion with and without moon-pool under the same wave condition, it is found that the

moon-pool actually introduces dissipations due to the internal fluid motion inside and near the moon-pool. This dissipation reduces the crest value of the pitch motion and damped the motion in the de-focusing process. But it has negligible effect on the heave motion, which is dominated by potential effects.

ACKNOWLEDGEMENT

This research was supported by the Engineering and Physical Sciences Research Council (EPSRC), U.K. Project: A Zonal CFD Approach for Fully Nonlinear Simulations of Two Vessels in Launch and Recovery Operations, under Grant No. EP/N008839/1.

REFERENCES

Berberovic, E, Hinsberg N V, Jakirlic, S, Roisman, I, and Tropea, C. (2009). "Drop impact onto a liquid layer of finite thickness: Dynamics of the cavity evolution ", *Physical Review E*, Vol. 79.

Faltinsen, O M, Rognebakke, O F and Timokha, A N. (2007). "Two-dimensional resonant piston-like sloshing in a moonpool ", *Journal of Fluid Mechanics*, Vol. 575, pp. 359–397.

Fredriksen, A G, Kristiansen, T and Faltinsen, O M. (2014). "Experimental and numerical investigation of wave resonance in moonpools at low forward speed.", *Applied Ocean Research*, Vol. 47, pp. 28–46.

Fredriksen, A G, Kristiansen, T and Faltinsen, O M. (2015). "Wave-induced response of a floating two-dimensional body with a moonpool ", *Philosophical Transactions of the royal society A*, Vol. 373.

Higuera, P, Lara, J L and Losada, I J. (2013). "Realistic wave generation and active wave absorption for Navier-Stokes models. Application to OpenFOAM. ", *Coastal Engineering*, Vol. 71, pp. 102–118.

Hu, Z Z, Causon, D M, Mingham, C G and Qian, L. (2011). "Numerical simulation of floating bodies in extreme free surface waves. ", *Natural Hazards and Earth System Sciences*, Vol. 11, pp. 519–527.

Hu, Z Z, Greaves, D and Raby, A. (2016). "Numerical wave tank study of extreme waves and wave-structure interaction using OpenFoam. ", *Ocean Engineering*, Vol. 126, pp. 329–342.

Palm, J, Eskilsson, C, Paredes, G M and Bergdahl, L. (2016). "Coupled mooring analysis of floating wave energy converters using CFD ", *International Journal of Marine Energy*, Vol. 16, pp. 83–99.

Qian, L, Mingham, C, Causon, D, Ingram, D, Folley, M and Whittaker, T. (2005). "Numerical simulation of wave power devices using a two-fluid free surface solver. ", *Modern Physics Letters B*, Vol. 19, pp. 1479–1482.

Ransley, E, Greaves, D, Raby, A, Simmonds, D and Hann, M (2017). "Survivability of wave energy converters using CFD ", *Renewable Energy*, Vol. 109, pp. 235–247.

Ransley, E., Yan, S., Brown, S., Mai, T., Graham, D., Ma, Q., Musiedlak, P.-H., Engsig-Karup, A. P., Eskilsson, C., Li, Q., Wang, J., Xie, Z., Sriram, V., Stoesser, T., Zhuang, Y., Li, Q., Wan, D., Chen, G., Chen, H., Qian, L., Ma, Z., Mingham, C., Causon, D., Gatin, I., Jasak, H., Vukevi, V., Downie, S., Higuera, P., Buldakov, E., Stagonas, D., Chen, Q., Zang, J., Greaves, D. (2019). "A blind comparative study of focused wave interactions with a fixed FPSO-like structure (CCP-WSI Blind Test Series 1) ", *International Journal of Offshore and Polar Engineering*, in press.

Yu, Y H and Li, Y. (2013). "Reynolds-Averaged Navier-Stokes simulation of the heave performance of a two-body floating-point absorber wave energy system. ", *Computers and Fluids*, Vol. 73, pp. 104–114.